Impact of Body Mass Index on Ultrawideband MIMO BAN Channels – Measurements and Statistical Model

Seun Sangodoyin, *Student Member, IEEE*, and Andreas F. Molisch, *Fellow, IEEE*

***Abstract*—Wireless Body Area Networks (BANs) have many important applications such as wearable communication devices and Internet-of-Things (IoT). Wireless propagation in on-body channels has been measured and modeled in the past. However, a crucial element that is usually ignored is the impact of the body size of the user – a 50 kg person obviously creates a different on-body channel than a 150 kg person. The *status-quo* 'one-size-fits-all' approach to channel characterization in BAN is thus incomplete. In this paper, we provide a detailed description of a propagation measurement campaign that employs a self-developed 4×4 Ultrawideband (UWB) Multiple-Input-Multiple-Output (MIMO) array channel sounding system to perform BAN channel sounding both in an anechoic chamber and indoor laboratory environments. A total of 60 human subjects were investigated in our work. These human subjects had widely varying Body Mass Index (BMI) values, which were grouped into three different categories, i.e., 20 *per* BMI category. Various propagation properties such as path gain, frequency-decay factor, shadowing gain, rms delay-spread, amplitude-fading and spatial correlation are extracted for each on-body channel under consideration. A comparison of statistics among the BMI categories reveals considerable differences emphasizing the fact that the aforementioned propagation properties are BMI dependent. Parameters such as path gain showed a monotonic decrease across the BMI categories with values ranging from 1-2 dB to almost 13 dB in some channels. This paper proposes a propagation channel model for the BMI dependent parameters and validates that it can reproduce the measured channel capacities.**

***Index Terms*—Body area network, body mass index, ultrawideband (UWB), statistical channel modeling, wireless propagation measurements.**

I. Introduction

In recent years, there has been an increased interest in Wireless Body Area Networks (BANs) because of their potential application in areas such as healthcare monitoring, surveillance and sports. Vital medical information of patients such as body temperature, heart rate and blood pressure can be obtained through biomedical sensors attached to the human body and wirelessly transmitted to a hub node (typically a cellphone) carried on the body [3]. Some of these sensors have already started to permeate the market in the form of pulse monitoring gloves, daily-exercise tracking wristbands and other wearable IoT devices. Additional devices, particularly in patient monitoring, are expected to emerge in the near future.

Seun Sangodoyin and A.F. Molisch are with the Department of Electrical Engineering, University of Southern California (USC), Los Angeles, CA 90089-2560 USA. Part of this work will be presented at VTC 2017 [1] and Globecom 2017 [2].

Ultrawideband (UWB) radio technology has been considered over the years as a promising candidate to enhance communication and localization in scientific, military, and industrial applications [4]–[7]. UWB signals are defined as either having more than 20% relative bandwith or more than 500 MHz absolute bandwidth [8] and are permitted to operate in the 3.1-10.6 GHz frequency band by the Federal Communications Commission [9] in the USA, while occupying 4.2-4.8 and 6-8.5 GHz bands in Europe, and 3.4-4.8 and 7.25-10.25 GHz bands in Japan [10]. UWB radio, due to its low power, high data rate, and robustness to fading has been suggested as the technology of choice for implementing BANs. Also, recent suggestions for improving BAN communications includes the use of Multiple-Input-Multiple-Output (MIMO) antennas to increase channel capacity [11] and robustness of the channel to fading [12].

In order to develop any reliable wireless system, it is essential that the channel in which the system will operate be characterized. Hence, comprehensive and realistic characterization of the on-body channel with a *realistic* model is essential.

It has been established through theoretical and practical investigation that the characteristics of narrowband and UWB channels are remarkably different [13]–[19]. Furthermore, in BANs, electromagnetic (EM) waves transverse the human body either via surface waves or diffraction mechanisms [12] and it is expected that the human body tissues will have a significant effect on the propagation especially when various body types (with different dimensions and tissue properties) are considered [20]. The Body Mass Index (BMI) is a measure of human body fat based on height and weight [21], [22] and can thus be anticipated to be a contributing factor to the characteristics of any on/off body wireless propagation. For medical applications, modeling the BAN on people with very high BMI is particularly important, since it is exactly this user group for whom medical BANs are especially relevant. However, most previous measurements and models considered test subjects with BMI < 25.

A. Related works

A number of papers [20], [23]–[49] in the literature have provided BAN models in the cm (below 10 GHz) frequency range.[1] These models range from narrowband to ultrawide-

[1]There are also models for mm-wave BAN channels; due to the significantly different propagation characteristics in that frequency range, we do not survey them here.

band and were derived either analytically, through numerical simulation or by actual measurements.

We can categorize existing results as:

- Narrowband models: Refs. [23]–[34] provide path gain models for propagation along/around the human body. These papers are based on analytical computation [23]–[28], numerical simulation [29], measurements with phantoms [30], measurements with human test subjects in an anechoic chamber [31], [32], indoor environment [33] and outdoor environment [34]. The most common frequency band for those measurements is 2.45 GHz [23]–[27], [30], [32]–[34] although 915 MHz [28] and 4.5 GHz [31] have been measured as well. A Finite-dimension time-domain (FDTD) simulation was done to develop BAN models at 400 MHz and 900 MHz in [29]. Narrowband static and dynamic measurements were conducted around 402, 900 and 2400 MHz frequency bands in [46]. These measurements made use of 20 human test subjects – both male and female. Also, a dynamic characterization of BAN communication channel at 2.4 GHz was conducted on 8 adult subjects in [47]. Narrowband measurements were conducted at 2.36 GHz using 5 adult test subjects performing 'everyday' activity in [48] while 3 adult subjects were used for narrowband measurement at 2.36 GHz in [49]. An open-access database, which contains hundreds of hours of all narrowband measurements conducted in [46]–[49] can be accessed in [50].
- Ultrawideband models: Refs. [20], [35]–[42] also provides pathloss models. Analytical derivations are provided in [39], numerical simulations are done in [20] while other papers were based on measurements in anechoic chamber [36], [38], [40] and indoor/office are provided in [35]–[37], [40]. The frequency bands used varies from 3-6 GHz in [35], [37] to 2-8 GHz in [38] and 3-10 GHz in [40], [44], [45].

Most of the above models, irrespective of the frequency band, are based on measurements or analysis on a single person or single phantom with the exception of [46]–[50], in which narrowband measurements were conducted on a larger sample size of test subjects. Furthermore, [41] analyzed the difference between propagation characteristics of three people with different weights. The measurement was conducted in the UWB frequency band of 3-5 GHz in an anechoic chamber, however the number of samples measured is too small to render the results statistically significant. [43] studied the effects of body shape and gender on BAN by conducting measurements on a total of 16 people (8 males and 8 females), however this was done for a narrowband channel (centered at 2.36 GHz). [42] conducted UWB measurements in the 3-10 GHz frequency band using 8 different human body sizes and shapes. This was done using a small sample size and also only the pathloss analysis was provided in the paper. We are unaware of any *ultrawideband* measurement-based model that characterizes the propagation channel responses based on the BMIs of a number of people sufficiently large to render results statistically significant.

B. Contribution

As can be seen from the literature review above, there exist, to the best of our knowledge, no measurements detailing *ultrawideband MIMO* BAN channels with a large sample size of human subjects that allow analysis of different BMI categories in an anechoic and indoor environment. In this paper, we remedy this by investigating the impact that BMI has on UWB-MIMO BAN channels. The contributions of this paper can be summarized as follows:

1) We provide an extensive report on the channel measurement campaign that employs our UWB MIMO array system to perform the BAN propagation channel measurement both in an anechoic chamber and indoor laboratory environments.
2) We provide estimates and statistics of extracted propagation channel parameters such as path gain, frequency-dependency coefficient of the path gain, shadowing gain, rms delay-spread, amplitude-fading and spatial correlation coefficient.
3) We propose a UWB MIMO BAN propagation channel model that takes the BMI of various people into consideration. The model is validated by comparing derived MIMO capacity values to those of the original measurements.
4) We provide an implementation recipe, which can be used to simulate BAN channels.

C. Organization

This paper is organized as follows. Section II describes the measurement environment while section III describes the measurement setup used in this campaign. Limitations of our study are extensively discussed in section IV. Data evaluation procedure and results are discussed in section V. The model implementation recipe is provided in section VI, while the model validation is presented in section VII. Conclusions are inferred in section VIII.

II. Measurement Environment

The measurements were conducted at the UltRa Lab facility [51] located at the University of Southern California (USC) in Los Angeles, CA, USA. The experiments were performed in both an anechoic chamber and indoor lab environments, which are shown in Figs. 1(a) and 1(b) respectively. The anechoic chamber is a 9.1 x 4.6 x 4.6 m Radio Frequency (RF) shielded room, which serves as a controlled environment with no reflections while the indoor lab is a 13.1 x 15.2 x 6.0 m room mostly populated with plastic chairs, computers, metallic workbench (labeled A) and two metallic pillars (labeled B), and also houses the anechoic chamber.

The human subject was positioned on a floor tile (labeled F) in the indoor lab while a platform (labeled P in Fig. 1) was used in the anechoic chamber. Additional details about the measurement environment are presented in [1].

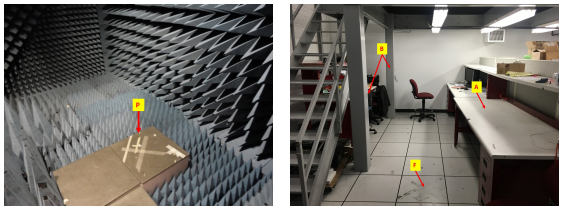

(a) (b)

FIG. 1: (a) anechoic chamber (b) indoor lab environment in the Ultralab at USC

Item	Manufacturer	Model No.
VNA	Agilent	8720ET
TX/RX RF switch	Pulsar Microwave	SW8RD13
coaxial cables	RF Industries	RFW-5950-96
UWB antennas	XY	XY3

TABLE I: Hardware used in the channel measurement

Parameter	Setting
Bandwidth	8 GHz (2 - 10 GHz)
Center frequency, f_c	6 GHz
Transmitted Power	-10 dBm
Total number of Channels	16
Number of sub-carriers	801
delay resolution	0.125 ns
Frequency resolution	9.98 MHz

TABLE II: Measurement parameters

Channel	Location
1	Front-to-Front (F2F)
2	Front-to-Shoulder (F2S)
3	Front-to-back (F2B)
4	Front-to-Hip (F2H)
5	Hip-to-Shoulder (H2S)
6	Hip-to-Back (H2B)
7	Hip-to-Leg (H2L)

TABLE III: On-body channels

III. MEASUREMENT SETUP

A task specific propagation channel sounder system was developed for our BAN measurement campaign. Fig. 2 illustrates our setup. The measurements were performed in the frequency domain using a vector network analyzer (VNA, Agilent 8720ET) for a stepped frequency sweep conducted for 801 frequency points within a range of 2-10 GHz. A 4-element switched arbitrary antenna array configuration (includes a combination of linear and/or rectangular) was used at both the TX and RX ends with an in-house developed XY3 omni-directional antennas [52]. The antennas were placed 7.5 cm apart in the linear array configuration in most instances while switching between array elements was performed by Pulsar Microwave (SW8RD13) RF switches [53]. A list of all equipment is given in Table I while all parameter settings for the channel measurement are shown in Table II. An extensive description of the channel sounding setup has been provided in [1].

Different on-body channels measured in our campaign are listed in Table III, while antenna placements on the body for these channels are shown in Figs. 3(a) to 3(g). A total of 60 male subjects with ages 18 years or older with various BMIs were considered. We could not conduct experiments with female subjects since no female research personnel qualified to work on this Instituitional Review Board (IRB) - approved project were available to work with female test subjects. The male test subjects were categorized according to their BMI values following a conventional medical classification [54] as shown in Table IV. The recruited subjects were later grouped such that there were 20 candidates *per* BMI category.

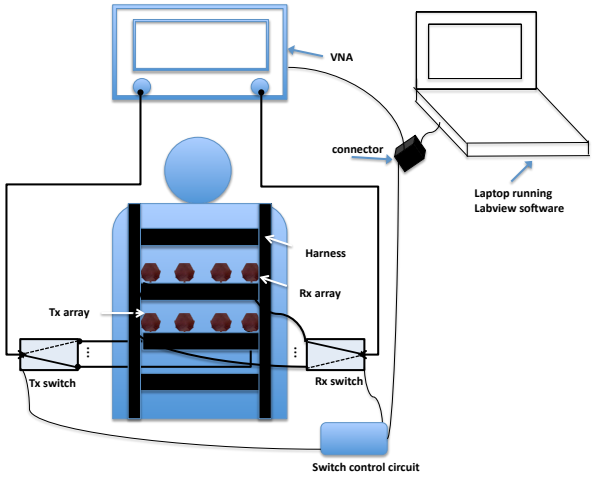

FIG. 2: UWB BAN measurement setup with harness on the body

Category	BMI Value	Classification
1	18.5-24.9	normal
2	25-29.5	overweight
3	$\geq$ 30	obese

TABLE IV: International classification according to BMI

A key assumption for our measurement is that the channel is *static*, which is fulfilled if there are no posture variations/ movements from the human subject or moving scatterers in the environmental. We thus made sure of this in our experiment. We made sure there were no moving scatterers in the vicinity of our measurement setup, and also monitored and instructed all test subjects to keep still while the measurements were being conducted.

IV. LIMITATIONS OF OUR STUDY

While this study is, to the best of our knowledge, the first of its kind (see Sec. I.A), the limited population used in our study, the use of BMI as a suitable measure for categorizing human body sizes and our choice of channel configuration and measurement environment merits a discussion.

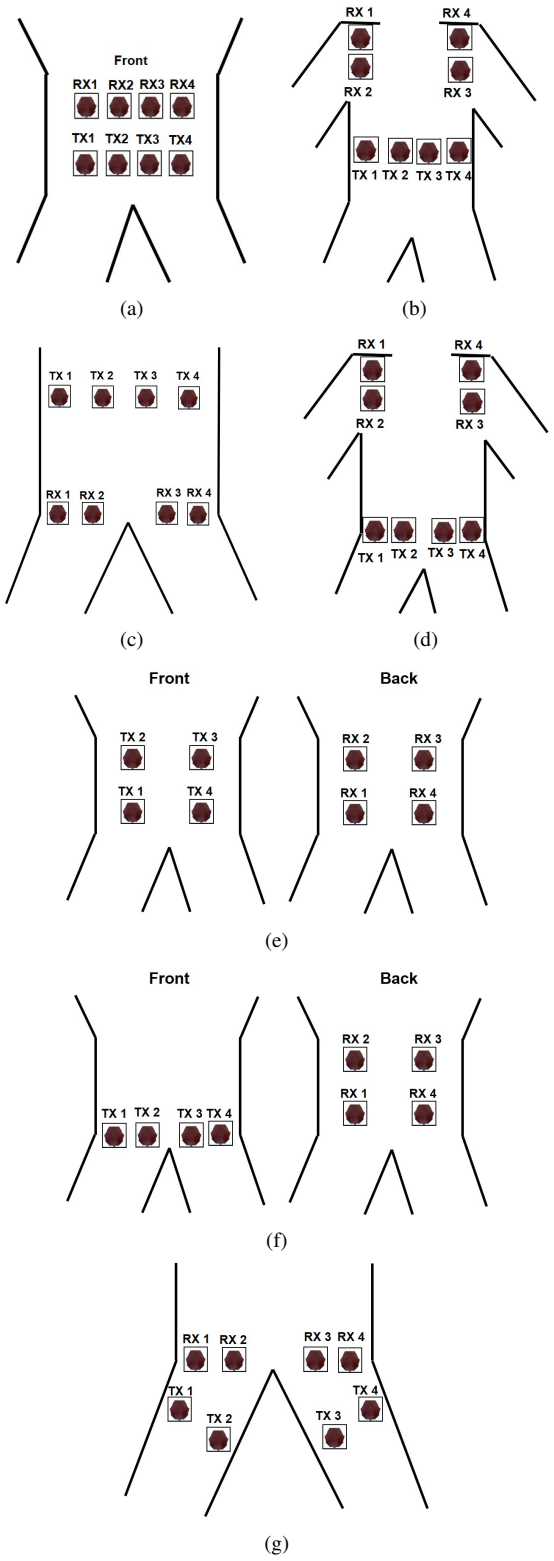

FIG. 3: (a) F2F (b) F2S (c) F2H (d) H2S (e) F2B (f) H2B (g) H2L

A. Limitation of population

One issue is the limited number (60) of test subjects. Obviously, a larger number would result in a better statistical viability of the model, but, the number of test subjects is limited both by difficulties in recruiting, and the time effort of measurements (see below). Furthermore, the current number gives reasonable reliability (see Sec. VI.A).

A more serious constraint is the limited *diversity* of the test population, specifically, our experiment used male subjects between the ages of 18 and 24. It can be expected that in particular women, with an inherently different body shape, and children under the age of 18 (with unusual body shapes during spurts of growth) could lead to significantly different results. However, extending the test population was not possible for two reasons: (i) having a statistically significant number in each of the mentioned population groups would mean at least tripling the number of measurements, leading to an impractical time effort (just the measurements reported here extended over a year, with the measurement on each test subject taking three hours, and considerable coordination effort to accommodate the volunteer test subjects). Furthermore, since we had no female IRB (Institutional Review Board)-qualified researcher on our team, we could not measure on female test subjects; and measuring with underage test subjects creates obvious permission issues.

To provide a comprehensive channel model that factors in a larger and more diverse population, additional channel measurements will need to be done. We encourage other research using the population groups not considered in this work to serve as a complement to our current work. Our setup and analysis as described in Secs. III & V will easily transfer to other groups/subpopulation of test subjects.

B. Limitation of BMI as a measure

The debate over the suitability of the BMI as a measure for quantifying the human body fat has been going on for a while and has been critically discussed in different works. While a lot of works such as [55], [56], [57] and [58] have oppposed the use of BMI as a valid measure for obesity, some works such as [59] and [60] have supported it.

We can categorize the differing opinions as:

- Opposed: Ref. [55] tested the accuracy of the BMI by comparing the adiposity status defined by BMI and dual-energy X-ray absorptiometry (DXA) in a large population. The conclusion of the work was that BMI misclassified adiposity status in approximately one-third of women and men compared with DXA. [56] also inferred that the accuracy of BMI in diagnosing obesity is limited, particularly for individuals in the intermediate BMI ranges, in men and in the elderly. [57] stated that BMI has various deficiencies as a measure of obesity and is an indirect measure of body fat when compared with more direct approaches such as bioelectrical impedance. Moreover, BMI does not necessarily reflect the changes that occur with age in a population. The proportion of body fat increases with age, whereas muscle mass decreases, but corresponding changes in height, weight and BMI may not reflect changes in body fat and muscle mass. [58] stated that consideration of changes in body composition rather than BMI should be used as a measure for determining obesity since weight variations have a bigger

impact on the BMI values even when the individual's height remains the same, which is especially common in adults.

- Support: In analyzing the measure of obesity and cardiovascular risk among men and women, [59] compared the waist-to-height (WHtR) ratio and BMI and concluded that BMI remained the most clinically practical measure of adiposity. [60] argues for the use of BMI as the principal and universal measure of obesity. [58] in contrast to its eventual assertion, stated that in a large population, BMI provides a useful surrogate index of obesity because it corrects for individuals who are heavy by virtue of the fact that they are also tall and that while BMI provides no information regarding the composition of the weight, or its distribution, it does not matter so much when the study is conducted on a large population.

Many other works (not mentioned here for space reasons) have provided various refinement of the BMI. In addition to the contrasting opinions in different works, it suffices to recall that the BMI is essentially height divided by weight. In adults, height is a fixed quantity [2], so BMI serves as a proxy for weight. In children/adolescents, both height and weight are variable, thus a much more diverse range of body types can be observed for a given BMI. Also, BMI has limitations not only on quantifying body fat but also composition (muscle vs fat as well as where the body fat is located). In a 'very large-framed' or muscular person, BMI may overstate body fat, while conversely it may understate body fat for a 'very small-framed' person, someone with little muscle mass, or an individual with excess body fat around the belly or midsection with very small limbs.

We use BMI for categorizing different body sizes in BAN propagation channel measurements and model for the following pragmatic reasons: (i) it provides a single-parameter description of human body shape. This is vital for this measurement campaign, because a description with a larger number of parameters would need a larger number of test subjects to obtain statistically viable results; yet for practical reasons a significant increase in that number of subjects is not feasible as discussed above. (ii) it can be measured in a standardized way (as opposed, e.g., to torso circumference), and cheaply (as opposed, e.g., to DXA). (iii) it is available for a very large population group since weight and height is measured at every doctor's visit and often at home. Perhaps most importantly, our measurements demonstrate that the standard deviation of channel parameters, such as path gain within each BMI category, is (slightly) less than the deviation between different categories as shown in the probability distribution functions (PDFs) plotted in Figs. 4(a) and 4(b). This demonstrates that the BMI is a *relevant* metric for the impact of body shape on radio propagation.

C. Limitation due to channel configuration and environment

On-body propagation channels measured in this work can be categorized into Line-of-sight (LOS) channels (e.g., F2F, F2H, F2S) and Non-line-of-sight (NLOS) channels (e.g., F2B, H2B). It is important to note that in on-body propagation, the term "LOS" and "NLOS" channels are only valid for *static* measurements such as the ones presented in this paper. As stated in [61], these terms are not valid in a *dynamic* scenario as body movement would significantly change the channel – obscuring the distinction between these two types of channels. Also, some of the parameters extracted in this work such as shadowing, amplitude fading and delay dispersion (to be discussed in subsequent sections) are all empirically determined in a *static* scenario.

[2]Note that the height of the test subjects used in our work ranges from about 160 to about 187 cm.

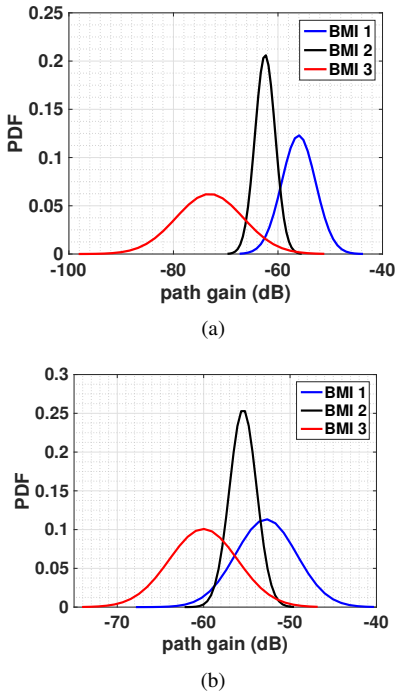

(b)

FIG. 4: PDF of the path gain in the (a) H2S in the anechoic chamber (b) F2S channels in the indoor lab

Due to the amount of effort involve in this type of measurement campaign and the configuration of our measurement setup, some channels such as TX or RX at lower leg or lower arm to other parts of the body were not measured. This could prove insightful for the UWB wireless BAN modeling, we hope any future research conducted in this field would take these channels into consideration to complement the results provided in this paper.

One important conclusion from the results of the current measurements is that they provide a quantitative estimate of the BMI influence in two extreme environments with no (anechoic chamber) or very rich (indoor lab) scattering. BAN channel measurements results conducted in other real-world environments are anticipated to lie between those extremes. It would indeed be interesting to measure the BMI impact in a range of other environments as well. The logistics and the sheer time effort of such measurements would have been prohibitive in the current campaign, but we hope that this paper can encourage studies of other researchers along those lines.

V. Data Evaluation and Results

The transfer function of each on-body channel can be represented as $H_{i,j,k,z,q,\psi,\xi}$, where $i \in [1,2,...,I=4]$ and $j \in [1,2,...,J=4]$ denote the TX and RX antenna position indices within the array, $k \in [1,2,...,K=801]$ represents the frequency points, $z \in [1,2,...,Z=7]$ is the type of on-body channel measured (see Table III), $q \in [1,2,...,Q=20]$ represents the index of people within a BMI category, $\psi \in [1,2,...\Psi=3]$ indicates the BMI categories, and $\xi \in [1,...,\Xi=2]$ represents the environments with $\xi=1$ as the anechoic chamber and $\xi=2$ as Indoor Lab environment, respectively. The transfer function $H_{i,j,k,z,q,\psi,\xi}$ was transformed to the delay domain by using an inverse Fourier transform and a Hanning window (to reduce side-lobes). The resulting impulse response is denoted as $h_{i,j,n,z,q,\psi,\xi}$, using similar index parameters representation as those of the transfer function with the exception of the frequency bin index changed to $n \in [1,2,...,N=801]$, where n indicates the delay bin index. The instantaneous power-delay profiles (PDP) are derived from the impulse responses by taking the magnitude squared ($P_{i,j,n,z,q,\psi,\xi} = |h_{i,j,n,z,q,\psi,\xi}|^2$) of the impulse response. The influence of small-scale fading is reduced by averaging the PDP over all MIMO channels so as to obtain the average power-delay-profile (APDP) as shown in (1). Sample APDP plots obtained from some of the channels in the BMI categories are shown in Figs. 5(a) & 5(b) below.

$$\hat{P}_{n,z,q,\psi,\xi} = \frac{1}{I}\frac{1}{J}\sum_{i=1}^{I}\sum_{j=1}^{J} P_{i,j,n,z,q,\psi,\xi} \tag{1}$$

To minimize the influence of noise in our data evaluation, we implemented a noise thresholding filter that sets all APDP samples whose magnitudes are below a certain threshold to zero. The threshold value is chosen to be 6 dB above the noise floor of the APDP [13]. Finally, a delay-gating filter was implemented for the anechoic chamber measurements only, which eliminated MPCs with an excess runlength (difference between runlength and Euclidean distance between TX and RX) larger than 4 m. The value 4 m was chosen because there were no observable reflector/scatterer that could cause a MPC with such a large excess runlength in the on-body channels.

In our data evaluation, we discuss the mode-of-propagation of MPCs in on-body channels, path gain, shadowing, delay dispersion, amplitude fading and spatial correlation. Extraction procedure and results for each of aforementioned parameters are discussed in subsequent sub-sections.

A. Mode of propagation of MPCs

In BAN, the Mode of Propagation (MOP) of an electromagnetic (EM) wave around the body has been classified as either through-body penetration or via creeping waves on the surface of the body, diffraction around the body or as a result of reflections in the environment [29], [62], [26], [35], [28]. While different on-body channels have different primary propagation mechanisms, subsequently received MPCs could stem from a combination of various MOPs. For example, the F2F channel in an indoor lab environment, as shown in Fig. 3(a) and APDP shown in Fig. 5(a), is more likely to be dominated by the creeping waves on the surface of the body while occurence of other MPCs is as a result of on-body and indoor reflections [35], [63]. For the F2B channel (see Fig. 3(e)), it can be deduced from the APDP (shown in 5(b)) that the first strongest peak corresponds to the MPC diffracted around the human body while the second strongest peak is mainly the result of ground reflection and subsequent MPCs are due to reflections in the environment. This characterization of the APDP from the F2B channel had been previously mentioned in [35]. It is important to note that the general shape of the APDP was the same at a particular on-body channels in the different BMI categories, which simply implies a common mode of MPC propagation within a channel irrespective of the body type.

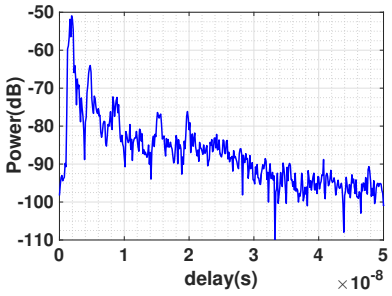

(a) APDP of F2F Channel

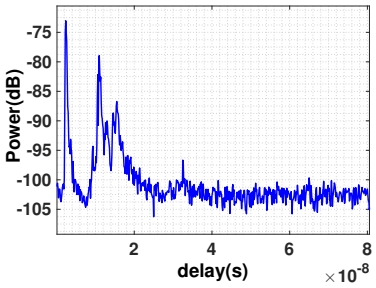

(b) APDP of F2B Channel

FIG. 5: APDP from sample measured channels in the indoor lab environment

B. Path gain Analysis

In the literature, path gain in narrowband channels is usually modeled as being dependent on distance only; while path gain in the UWB channel exhibits both distance and frequency dependency [19], [63] and is written as

$$\mathrm{G_L}(f,d) = \frac{1}{\Delta f}\cdot \mathrm{E}\left\{\int_{f-\Delta f/2}^{f+\Delta f/2} \left|\mathrm{H}(\widetilde{f},d)\right|^2 d\widetilde{f}\right\}, \tag{2}$$

where $\mathrm{H}(\tilde{f}, d)$[3] is the channel transfer function. $\mathrm{E}\{\cdot\}$ is the expectation taken over the fading.[4] The frequency range, Δf is chosen small enough so that diffraction coefficients, dielectric constants, etc., can be considered constant within that bandwidth. For our measurement, Δf is chosen to be 200 MHz, which is sufficient to average out frequency-selective fades.

As a consequence of the nature of our work, there are no distance dependencies of path gain for each channel since the channels were measured at a fixed TX-RX separation. The path gain can be expressed as

$$\mathrm{G_L}(f, d_0) = \mathrm{G_0} \cdot \mathrm{X}_\sigma \cdot \mathrm{G_L}(f), \tag{3}$$

where $\mathrm{G_0}$, X_σ and $\mathrm{G_L}(f)$ are the average path gain at a fixed distance ($d = d_0$), shadowing gain and frequency-dependent path gain respectively. These parameters will be discussed in detail subsequently.

1) Fixed distance path gain: For each test subject, we compute the local mean power ($\mathrm{M}_0^{z,q,\psi,\xi}$) as shown in (4))

$$\mathrm{M}_0^{z,q,\psi,\xi} = \sum_{n=1}^{N} \hat{P}_{n,z,q,\psi,\xi}, \tag{4}$$

from which we then compute $\mathrm{G_0}$ as

$$\mathrm{G}_0^{z,\psi,\xi} = \frac{1}{Q} \sum_{q=1}^{Q} \mathrm{M}_0^{z,q,\psi,\xi}. \tag{5}$$

Values for $\mathrm{G_0}$ obtained from our measurements are provided in Table V. Sample cumulative distribution function (CDF) plots for $\mathrm{M_0}$ in different BMI categories and environments for example channel F2H are shown in Figs. 6(a) and 6(b).

It can be observed from Table V that $\mathrm{G_0}$ values differ by only about 2 dB between BMI 1 and BMI 2 while the difference to BMI 3 is much larger, namely 3-13 dB. It is intuitive that the path gain is lower for BMI 3, since more body mass needs to be transversed with exposure to more body tissue, which will likely attenuate the transmitted signal. Also, for channels on the front of the body, protruding bellies of the BMI 3 subjects decrease the average path gain while the variation (shadowing) is increased. Path gain in the two different environments (anechoic chamber and indoor lab) are similar except for the "Non-Line-of-Sight (NLOS)" channels (F2B, H2B), where path gain values in the indoor lab environment are actually higher than those of the anechoic chamber. This can be explained by the fact that additional propagation paths (from the TX via scatterers in the environment to the RX) can be more efficient than the creeping/diffracted waves that constitute the only propagation path in the anechoic chamber.

2) Frequency-dependent path gain: The frequency dependency in the BAN UWB channel arises primarily from the frequency dependency of the antenna power density and gain variation [64], [65], the tissue constituents of the human body, and the physical propagation phenomena such as scattering and diffraction [66] in the channel.

Following [67], [68], we model $\mathrm{G}_L(f)$ as

$$\mathrm{G}_L(f) = \zeta \left(\frac{f}{f_0} \right)^{-2\kappa}, \tag{6}$$

where κ is the frequency decay factor, ζ is a normalization constant, f_0 is the center frequency. In our analysis, the average of the frequency-decay factors, extracted separately for each candidates in each BMI category is used for modeling κ. While [69] has shown that κ can be different for each multipath component, we use here (like most other papers describing frequency dependence) a bulk model because we did not have sufficient number of measurement points to extract it for each path separately. All extracted κ values are provided in Table V.

Although there has been some recent work done aimed at de-embedding the antenna effect from the on-body propagation channel [70], [71], it is important to note that any results in our analysis represent the behavior of the radio channel *including both the physical propagation channel (human body) and the antennas*. Different antennas with consequently different frequency dependent behavior could lead to significantly different results. All other measurement campaigns that do not

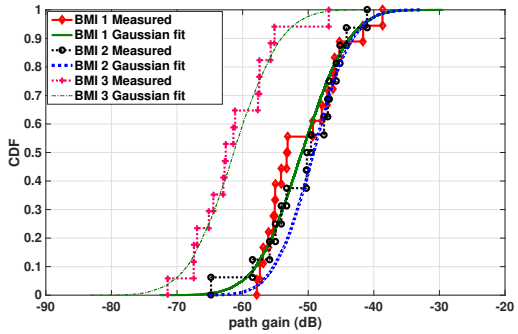

(a)

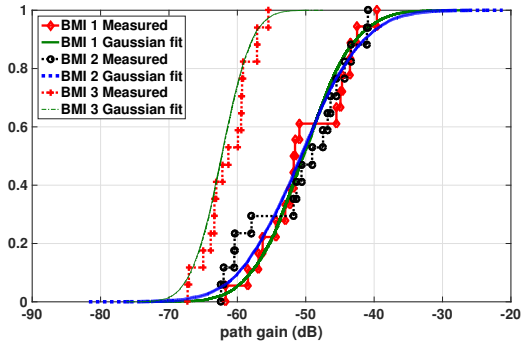

(b)

FIG. 6: Empirical CDF and corresponding Gaussian fit of path gain for F2H channel in (a) anechoic chamber (b) indoor lab environments.

[3]We have used the transfer function notation as stated in [63].

[4]Note that due to the nature of our setup, there is no large-scale fading created by movement along a trajectory; rather the "shadowing" variable introduced below describes as the different "realizations" the results on the different users. To simplify notation, we henceforth speak of "fading" when we mean small-scale fading arising from interference between multipath components

Average path gain, G_0 (dB)														
	F2F		F2B		F2H		F2S		H2B		H2L		H2S	
	Anec.	Ind.	Anec.	Ind.	Anec.	Ind.	Anec.	Ind.	Anec.	Ind.	Anec.	Ind.	Anec.	Ind.
BMI 1	-39.40	-40.78	-72.68	-63.62	-49.23	-50.69	-54.14	-55.63	-60.80	-58.61	-40.52	-41.14	-55.49	-61.29
BMI 2	-41.91	-41.66	-72.17	-65.98	-50.90	-50.18	-56.28	-56.43	-62.64	-61.21	-42.40	-41.69	-62.31	-62.16
BMI 3	-47.55	-45.76	-86.37	-74.57	-63.58	-62.32	-61.88	-61.68	-66.58	-65.44	-45.93	-49.64	-72.20	-71.26
Frequency-dependent decay factor (κ)														
BMI 1	1.05	1.06	1.21	1.22	1.20	1.22	1.28	1.25	1.23	1.20	1.03	1.18	1.31	1.48
BMI 2	1.04	1.05	1.31	1.36	1.21	1.21	1.29	1.30	1.30	1.16	1.23	1.26	1.42	1.54
BMI 3	1.04	1.13	1.86	1.57	1.46	1.43	1.43	1.38	2.03	1.88	1.40	1.59	1.50	1.92
Shadowing gain, σ_s(dB)														
BMI 1	2.69	4.55	8.57	6.65	5.88	7.12	5.26	5.61	6.67	7.04	5.24	4.48	3.20	4.00
BMI 2	3.50	4.21	5.54	3.77	5.61	6.06	5.13	5.34	7.21	2.91	4.06	6.11	2.90	5.33
BMI 3	4.27	2.55	2.90	5.88	5.22	3.54	3.07	3.40	8.07	3.16	3.16	1.90	4.37	2.59
mean rms delay-spread, $\mu_{\tau^{\text{rms}}}$ (dBs)														
BMI 1	-90.74	-86.93	-91.28	-84.68	-91.94	-85.97	-89.84	-84.81	-92.13	-83.81	-90.62	-87.12	-88.62	-81.32
BMI 2	-90.82	-86.25	-93.06	-84.39	-91.53	-87.02	-88.28	-82.03	-90.11	-84.14	-90.76	-87.23	-88.18	-81.83
BMI 3	-96.09	-86.22	-102.81	-86.10	-94.52	-85.78	-92.52	-76.66	-88.83	-80.13	-116.28	-87.01	-90.85	-81.38
std. dev rms delay-spread, $\sigma_{\tau^{\text{rms}}}$ (dBs)														
BMI 1	3.06	4.11	4.92	1.83	3.65	4.63	3.01	3.61	3.86	3.36	3.19	3.98	3.40	2.12
BMI 2	2.39	2.55	5.30	1.77	2.71	5.26	2.63	3.74	3.90	4.83	3.01	3.01	3.91	2.67
BMI 3	3.33	5.39	2.71	1.21	1.69	5.62	0.85	2.78	2.19	4.76	3.62	4.13	5.50	3.61
mean $\mathcal{K}$-factor, $\mu_{\mathcal{K}}$ (dB)														
BMI 1	2.30	2.05	2.01	2.13	2.82	1.24	1.12	1.31	2.28	0.94	2.10	3.10	1.80	0.92
BMI 2	3.06	2.88	3.11	3.21	2.69	1.69	1.31	1.02	-1.23	-0.80	1.80	2.90	-1.23	-1.20
BMI 3	3.66	2.78	4.72	1.91	1.70	2.14	1.21	1.43	2.53	1.03	2.40	1.10	-1.56	1.27
std. dev $\mathcal{K}$-factor, $\sigma_{\mathcal{K}}$ (dB)														
BMI 1	0.58	0.89	1.39	0.67	2.27	1.11	0.80	1.04	0.32	0.84	0.55	1.40	1.70	2.34
BMI 2	1.53	1.19	2.22	3.06	1.11	1.19	1.19	1.93	2.12	1.08	1.10	0.82	1.80	2.30
BMI 3	3.04	0.83	0.78	2.11	1.08	1.18	1.07	3.20	1.12	0.67	1.72	0.93	3.1	2.10

TABLE V: Parameters extracted for various channels and BMI categories

use calibrated antennas have the same limitation.

C. Shadowing

Shadowing gain (X_σ) accounts for the fluctuations of the received power for a given channel and environment type, as well as BMI category, between different test subjects. The standard deviation (std. dev) of shadowing gain computed from all channels and BMI categories in the anechoic and indoor lab environments are shown in Table V; it mainly ranges from 2.55 to 8.57 dB. There is very little difference between these std. dev values among BMI categories and the environments.

In generic UWB propagation channel measurements [72], [73], the shadowing gain has been characterized as a log-normal distribution $N(0, \sigma_s(\text{dB}))$. This distribution for the shadowing gain was also used in our work, even though the generating mechanism is different. The lognormal distribution was validated by matching the empirical data to some typical theoretical distribution such as lognormal, Nakagami, Rayleigh, Ricean, and Weibull. The Kolomogorov-Smirnov (K-S) hypothesis test was used to determine the goodness-of-fit of these distribution at 5% significance level (Table VI).

As can be observed from Table VI, the lognormal distribution gives the highest passing rate for both anechoic and indoor lab environments. This observation holds for all BMI categories and channels. A sample distribution for a select channel (F2F) is shown in Fig. 7.

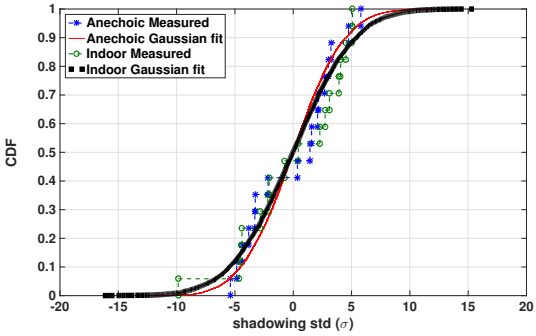

FIG. 7: Empirical CDF and corresponding Gaussian fit for the shadowing gain in the F2F channel of BMI 1 in both anechoic and indoor lab environments.

D. Delay Dispersion Statistics

The rms delay-spread, τ^{rms} is defined as the square-root of the second central moment of the normalized APDP. This parameter serves to compactly describe the effects of delay dispersion in multipath propagation environments [74]. The rms delay-spread was computed directly from the APDP as described in [75].

We found rms delay-spread to be lognormally distributed (with respect to the ensemble of subjects within a BMI category). The CDF plots in Figs. 8(a) and 8(b) show that

the logarithmic value of ${\tau^{\text{rms}}}_{z,\psi,\xi}$ (with respect to 1 s) is well approximated by a Gaussian distribution; this holds for all the other BAN channels measured in various environments as well. This was again validated with a K-S test using the same distributions and significance level as for the shadowing. Table VII compares the passing rate of the aforementioned distributions for a sample channel (F2H-BMI 1) in both anechoic and indoor environments. It can be observed from the result that the lognormal distribution has the highest passing rate. The statistical parameters (second-moment) for the rms delay-spread values (expressed in dB) for all BAN channels are shown in Table V. BMI 3 categories typically have the smallest τ^{rms} values. Also, as a consequence of the environment, comparing rms delay-spread values between BMI categories is more difficult in the indoor Lab environment as scattered and reflected MPCs drown out the impact of creeping or diffracted waves. Conversely, the measurements in the anechoic chamber show a stronger dependence on BMI, since there exist few or no reflections in the channel. Also, the rms delay-spread values in the indoor lab environment are larger than the anechoic due to the rich scattering environment. Impact of MPC delay dispersion on BAN or Personal Area Network (PAN) system performance have been studied in papers such as [76] and [77].

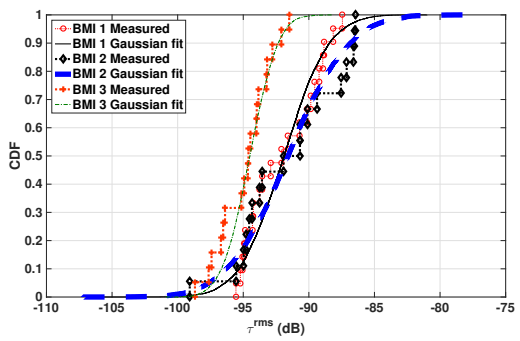

(a)

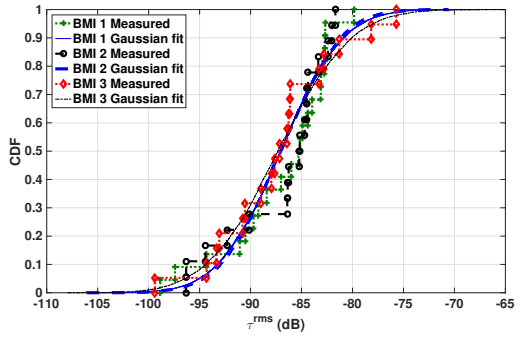

(b)

FIG. 8: Empirical CDF and corresponding Gaussian fit of τ^{rms} in the F2H channel in (a) anechoic chamber (b) indoor lab environment

Distribution	K-S (anechoic)	K-S (indoor)
Weibull	78.28	57.00
Rayleigh	16.17	15.23
Rician	16.17	15.23
Lognormal	98.37	89.36
Nakagami	27.87	36.59

TABLE VI: Passing rate of K-S test at 5% significance level for BMI 1 F2F channel

Distribution	K-S (anechoic)	K-S (indoor)
Weibull	55.16	45.24
Rayleigh	3.82	9.14
Rician	3.82	9.14
Lognormal	93.00	89.32
Nakagami	69.71	52.40

TABLE VII: Passing rate of K-S test at 5% significance level for τ^{rms} for BMI 1 F2H channel

E. Amplitude Fading Statistics

The variation in the received signal amplitude over the 4 $\times$ 4 MIMO UWB channel can be attributed to the small-scale fading (SSF) on the body. This variation stems from MPC interaction with local scatterers such as head, arm, etc (depending on the channel measured), which exist within the vicinity of the receiver.

Several channel measurements [13], [75], [78]–[81] have described the SSF statistics as either lognormal, Rician, Rayleigh or m-Nakagami distributed. In our work, the SSF statistics was found to follow a Ricean distribution. This was investigated by considering fading on sub-carriers in different sub-bands over MIMO sub-channels. The chosen sub-carriers in contiguous sub-bands are 200 MHz apart so to reduce the bias introduced by possible correlation between sub-carriers [82]. An ensemble of the amplitude at each such chosen sub-carrier and MIMO sub-channels are used in modeling the Ricean distribution. The $\mathcal{K}$-factor is essentially constant over frequency, as verified by computing $\mathcal{K}$-factor for 1-GHz sub-bands (not shown here for space reasons). The $\mathcal{K}$-factor parameter of the Ricean distriibution was computed using the method of moments as described by (1)-(9) in [83]. A distribution fit from sample measurement data is provided in Fig. 9 below. Also, a K-S hypothesis test at 5% significance level was used to determine a goodness-of-fit for the aforementioned empirical data as compared to typical theoretical distributions such as Rayleigh, Rician, Lognormal, Nakagami, and Weibull. Table VIII compares the passing rate of these tests for our measurement data. It is clear that the Ricean distribution has a much higher passing rate.

The $\mathcal{K}$-factor parameter of the Ricean distribution was found to be lognormally distributed over the ensemble of all subjects within a BMI category for each channel measured for different environments. First and second moment values for a logarithmic equivalent, i.e., Gaussian distributed $\mathcal{K}$-factor $\mathcal{N}(\mu_\kappa(\text{dB}), \sigma_\kappa(\text{dB}))$ statistics are provided in Table V. We did not observe a significant $\mathcal{K}$-factor dependency on BMI values in our analysis.

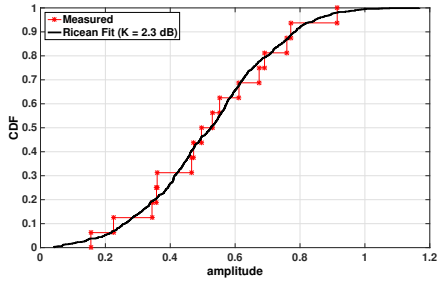

FIG. 9: Ricean distribution fit for small-scale amplitude fading in F2F anechoic channel

Distribution	K-S
Weibull	84.89
Rayleigh	58.43
Rician	98.50
Lognormal	75.78
Nakagami	92.58

TABLE VIII: Passing rate of K-S test at 5% significance level

F. Spatial Correlation

Correlation of the signals at different antenna elements could have an adverse effects on the channel capacity of a MIMO system. Correlation is influenced by the angular spectrum of the channel as well as the arrangement and spacing of antenna elements [84]. For antennas that have been spaced half a wavelength apart, a uniform angular power spectrum leads approximately to a decorrelation of incident signals. A smaller angular spread of the channel leads to an increase in correlation. For a given Signal-to-Noise Ratio (SNR), maximum capacity is achieved when the channel transfer matrix has full rank and the singular values of the MIMO channel matrix are equally strong. If the fading of the channel coefficients is correlated, this will lead to reduction in the MIMO system capacity.

We approximated the spatial correlation matrix of the non-LOS part of the channel (i.e., after the subtraction of the LOS component) channel as the Kronecker product of the spatial correlation matrix at the TX and RX sides such that

$$\mathbf{R} = \mathbf{R}^{\mathrm{TX}} \otimes \mathbf{R}^{\mathrm{RX}} \tag{7}$$

where $\otimes$ denotes that Kronecker product and the matrices $\mathbf{R}^{\mathrm{TX}}$ has as their entries the complex correlation coefficient $\rho_{j,i}$ between two sub-channels with ith and jth TX antenna element.[5] This approach is similar to what has been implemented for different wireless channels in the literature [85], [86], [87] and [88]; it is furthermore necessary in our case to obtain an ensemble over which the expectation can be taken. We note that even with this approximation, the ensemble size is on the low side. Furthermore, we do not model the dependence of the correlation on delay, but assume it is identical for all delay bins (note that we have already subtracted the impact of the LOS component, so that we only assume that the *diffuse* components are delay-independent). With this assumption, we can then use the ensemble of subcarriers (with similar constraints as in Sec. V-E), at all RX antennas, as the ensemble, thus greatly increasing the ensemble size and reducing random variations. It must be noted, however, that by the very nature of this process, we cannot extract delay dependence of the correlation matrix.

For the various on-body channels analyzed, the spatial correlation coefficients were usually approximately uniformly distributed between 0 and 0.5-0.6. For example, in the F2F channel (which can be considered a LOS channel - antenna arrangements on the human body are shown in Fig. 3(a)), the CDF plots of the spatial correlation between sub-channels at the TX and RX, respectively over an ensemble of human subjects within a BMI are shown in Figs. 10(a) and 10(b). A simplified approach was used in modeling $\mathbf{R}^{\mathrm{TX}}$ and $\mathbf{R}^{\mathrm{RX}}$ by having correlation coefficient value of 1 in the diagonal of the correlation matrix while all off-diagonal matrix values are set to 0.3. We compared this approach to a more complicated approach in which each correlation coefficient was modeled by a uniform random distribution (over the ensemble of test subjects), and the correlation between the correlation coefficients of one user were taken into account (thus ensuring, e.g., that ρ_{12} was always larger than ρ_{14}). We found that both the capacity distribution and the distribution of the eigenvalues in the two modeling approaches (the simple constant off-diagonal, and the more involved one) gave almost the same results, and were well aligned with the correlation coefficients as directly extracted from the measurements. We also compared to the simple i.i.d. assumption, but found significant differences in both the capacity distribution and eignevalue cdf.

We did not observe any impact of BMI on the correlation coefficient values. Given the fact that most of the sub-channel exhibit low correlation coefficient, it is fair to expect a high capacity value even for the LOS channels in all the environments. An extensive discussion on the MIMO channel capacity values obtained in our work has been presented in [2].

VI. IMPLEMENTATION RECIPE

During simulations, we aim to create a frequency-selective MIMO fading channel ($\bar{\mathbf{H}}$) with N_T transmit and N_R receive antennas for BAN channels. The channel realizations can thus be generated as follows:

1) Select an on-body channel, BMI category and environment desired.
2) Select a suitable frequency band and delay window for the simulation. Also, select appropriate sampling grid to create taps in delay.
3) From Table V, select corresponding values for G_0, κ and σ_{s} and then generate $\mathrm{G}_L(f, d_0)$ by using (3) .
4) Generate P_n for each delay tap using

$$P_n = \mathrm{G}_L(f, d_0) \cdot \eta \cdot e^{-\frac{\tau_n - \tau_0}{\alpha}} \tag{8}$$

where η is a normalization constant such that $\sum_{n=0}^{\infty} e^{-\frac{\tau_n - \tau_0}{\alpha}} = \frac{1}{\eta}$ and α is a realization of the τ^{rms}. The pdf of the rms delay-spread is lognormal; its parameters

[5] and vice-versa in the RX case

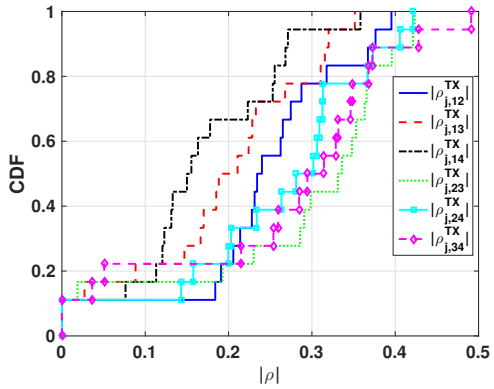

(a)

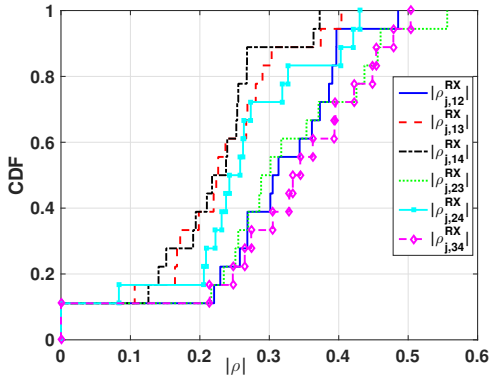

(b)

FIG. 10: Emprical CDF of the correlation magnitude for (a) TX array for BMI 1 in anechoic for F2F channel (b) RX array for BMI 1 in anechoic for F2F channel

are give in Table V. Note that this shape of the PDP is not necessarily the one that was observed in our measurements; however, due to the restriction on the number of scenarios we could measure, a more detailed modeling of the PDP is beyond the scope of the paper.

5) Compute the Fourier transform ($\mathbb{F}\{\cdot\}$) of P_n such that

$$P_f = \mathbb{F}\{P_n\} \tag{9}$$

6) Generate a matrix $\hat{\mathbf{H}}_{\text{LOS}}$ for the LOS component using (10) and (11).

$$\hat{\mathbf{H}}_{\text{LOS}} = \mathbf{a}(\text{p})\mathbf{a}(\text{q})^T \tag{10}$$

$$\mathbf{a}(\text{r}) = e^{-j\frac{2\pi}{\lambda}|\overrightarrow{\text{r}}_i - \overrightarrow{\text{r}}_j|} \tag{11}$$

where $|\overrightarrow{\text{r}}_i - \overrightarrow{\text{r}}_j|$ is the location vector of the array antenna elements

7) Generate a residual matrix $\hat{\mathbf{H}}_{\text{res}}$ as shown in (12).

$$\text{vec}(\hat{\mathbf{H}}_{\text{res}}) = \mathbf{R}^{1/2}\text{vec}(\mathbf{H}^w) \tag{12}$$

where the $N_T N_R \times N_T N_R$ matrix $\mathbf{R}^{1/2}$ is obtained by factoring the total correlation matrix $\mathbf{R}$, i.e., $\mathbf{R} = \mathbf{R}^{1/2}\mathbf{R}^{1/2}$. The spatial correlation matrix $\mathbf{R}$ can be generated using the simplified approach described in Sec. IV-F. $\mathbf{H}^{\text{w}}$ is a complex i.i.d white Gaussian random matrix.

8) Generate a linear equivalent of the $\mathcal{K}$ (dB) from the Gaussian distribution using corresponding moment values in Table V.

9) Generate a realization of the propagation channel $\tilde{\mathbf{H}}$ in (13) by combining all the parameters above.

$$\tilde{\mathbf{H}} = \sqrt{P_f}\left(\sqrt{\frac{\mathcal{K}}{\mathcal{K}+1}}\hat{\mathbf{H}}_{\text{LOS}} + \sqrt{\frac{1}{\mathcal{K}+1}}\hat{\mathbf{H}}_{\text{res}}\right) \tag{13}$$

10) Multiply $\tilde{\mathbf{H}}$ by $\left(\frac{f}{f_c}\right)^{-\kappa}$ to obtain $\bar{\mathbf{H}}$ as shown in (14)

$$\bar{\mathbf{H}} = \tilde{\mathbf{H}} \cdot \left(\frac{f}{f_c}\right)^{-\kappa} \tag{14}$$

VII. Model Validation

The model presented in this work was validated by using the channel capacity and by dividing each BMI category randomly into two subgroups, extracted parameters for each of the subgroups, and comparing these parameters.

A. Capacity Approach

For each channel measured, an equal power capacity [44] was computed by using the channel coefficients from $\tilde{\mathbf{H}}$. The CDF of the capacity (TX SNR = 68 dB) obtained from data generated synthetically from our model and that computed from the measurement data for each BMI category for the F2F channel are compared in Figs. 11(a)-11(c) below. The CDF was derived using an ensemble from candidates within each BMI categories.

Visually, it is clearly observable (from the CDFs plots in Figs. 11(a) to 11(c)) that the capacity results from the model does have a good fit to that obtained from the measured data. In addition to this visual confirmation, a maximum deviation ($D_{\text{v}} = \text{Maximum}_{\text{x}}|F_{\text{model}}(\text{x}) - F_{\text{empirical}}(\text{x})|$) value[6] metric, which describes how closely the model and the empirical data match was implemented. D_{v} is equivalent to the *Kolmogorov-Smirnov test statistic* and has been extensively discussed in [89]. The values of D_{v} between the CDFs for BMI 1, 2 and 3 as shown in Figs. 11(a) to 11(c) are small – confirming a good fit and have been provided in Table IX.

Category	D_{v}
BMI 1	0.18
BMI 2	0.12
BMI 3	0.16

TABLE IX: Maximum deviation D_{v} values for Capacity CDFs for BMI 1, 2, 3 F2F channels

B. Sub-group Analysis Approach

For each BMI category, we randomly divided the measurement data into two sub-groups (having equal number of candidates) and extracted parameters such as G_0 and mean

[6] where $F_{\text{model}}(\text{x}), F_{\text{empirical}}(\text{x})$ are the distributions obtained from model and the empirical data.

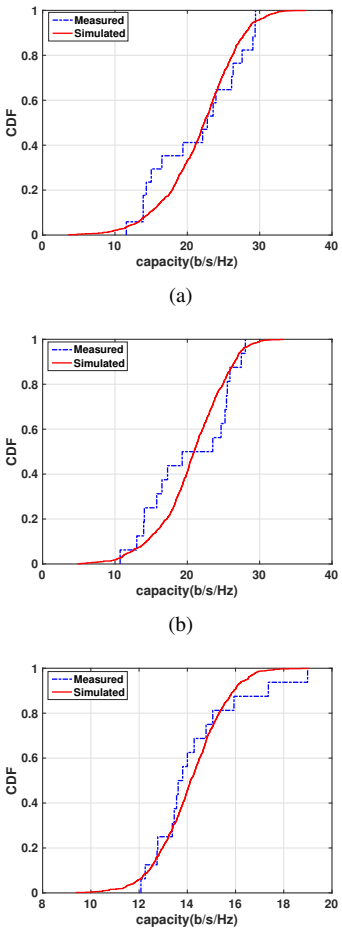

FIG. 11: Emprical CDF and model fit of capacity for (a) BMI 1 F2F (b) BMI 2 F2F (c) BMI 3 F2F

delay-spread τ^{rms} for comparison in the F2F, F2H and H2S channels. Similar parameters values between the two sub-groups, which are also in agreement with the overall results shown in Table V would corroborate the accuracy of our result irrespective of the data size used. These parameters are shown in Table X below.

It can be observed from Table X that the parameters from different sub-groups for these channels in the same environments are similar (with a few exceptions, e.g., G_0 for BMI 3 F2F, F2H Anechoic and H2S Indoor Lab) and are also close to values provided in Table V, which supports the notion that number of samples used in our analysis is in fact sufficient.

VIII. Summary and Conclusion

We conducted a BAN measurement campaign using a UWB MIMO (4 x 4) antenna array channel sounder setup for various on-body channels for different BMI categories in an anechoic chamber and indoor lab environments. We extracted parameters used for modeling a UWB BAN channel characteristics with respect to various BMI categories. A summary of our findings is presented as follows:

1) We observed that parameters such as path gain do in fact vary for different BMI categories. The path gain values were lower in BMI 3 than for BMI 1 and 2 by almost 13 dB in some channels.
2) Frequency-decay factor κ ranged from 1.03 to 1.92 and did not vary much over BMI categories. However, this parameter is notably a function of the antenna used in our measurement.
3) Shadowing gain was modeled as lognormal distribution with standard deviation values ranging from 2.5 to 8.5 dB. We observed that there were very little differences between the std. dev values among BMI categories and the environments.
4) The delay-spread statistics showed that the rms delay-spread values tends to follow a lognormal distribution, which is consistent with the previous literature. We observed that BMI 3 categories typically have the smallest τ^{rms} values. Also, τ^{rms} values are higher in the indoor lab environment than in the anechoic chamber.
5) The amplitude fading statistics was modeled using a Ricean distribution while the $\mathcal{K}$-factor parameter was found to be lognormally distributed over an ensemble of subjects and did not show any dependence on BMI category.
6) A Kronecker approach was used in modeling the spatial correlation of the MIMO channel. A low correlation was generally observed between the sub-channels. This implies that a high capacity value can be obtained with spatial multiplexing.
7) Based on these results, we provide a complete UWB MIMO BAN channel model and give a step by step modeling procedure. The results were validated by using MIMO capacity values as a comparison metric and also agreement between parameters extracted from sub-groups of the data at each BMI category.
8) It is important to note that the modeling technique used in this work is generic and can be adapted to any multi-paramater body composition metric (other than the BMI) in any future research.

Overall, it is clearly observable from the results and statistics presented in this paper that the propagation channel parameters for the UWB BAN channel does in fact differ for different BMI categories. The *status-quo* BAN models are incomplete, hence our work serves as either a complement to pre-existing models or a replacement. Details such as those provided in this work will be of great help for BAN systems design and simulation in various environments.

IX. Acknowledgment

The authors would like to thank Prof. Fredrik Tufvesson from Lund University, Sweden, for providing antennas used for an earlier version of the experiment. They would also like to thanks Phil Philip for helping with the preliminary setup, Dr. S. Niranjayan for helping with circuit design, Dr. Donna Spruijt-Metz for helping with the initial recruitment and Vishnu Ratnam for helping with the recruitment fliers. Finally, the authors would like to thank the USC Institutional

Anechoic - Average path gain, G_0 (dB)									
	F2F			F2H			H2S		
	BMI 1	BMI 2	BMI 3	BMI 1	BMI 2	BMI 3	BMI 1	BMI 2	BMI 3
Sub-group 1	-39.72	-43.57	-44.13	-50.90	-51.04	-65.36	-59.14	-65.04	-67.90
Sub-group 2	-40.60	-44.21	-51.44	-50.74	-51.51	-60.75	-60.89	-63.39	-68.01
Indoor Lab - Average path gain, G_0 (dB)									
	F2F			F2H			H2S		
	BMI 1	BMI 2	BMI 3	BMI 1	BMI 2	BMI 3	BMI 1	BMI 2	BMI 3
Sub-group 1	-42.60	-43.95	-47.02	-50.39	-51.35	-61.40	-60.17	-64.44	-73.10
Sub-group 2	-42.36	-43.40	-48.32	-48.80	-50.10	-63.59	-60.44	-62.30	-69.88
Anechoic - mean rms delay-spread, $\mu_{\tau^{\text{rms}}}$ (dBs)									
	F2F			F2H			H2S		
	BMI 1	BMI 2	BMI 3	BMI 1	BMI 2	BMI 3	BMI 1	BMI 2	BMI 3
Sub-group 1	-90.19	-91.02	-96.70	-91.81	-90.89	-94.37	-89.19	-88.44	-91.87
Sub-group 2	-90.50	-91.15	-95.48	-91.72	-92.38	-94.04	-88.35	-87.95	-90.15
Indoor Lab - mean rms delay-spread, $\mu_{\tau^{\text{rms}}}$ (dBs)									
	F2F			F2H			H2S		
	BMI 1	BMI 2	BMI 3	BMI 1	BMI 2	BMI 3	BMI 1	BMI 2	BMI 3
Sub-group 1	-87.88	-87.52	-86.14	-86.63	-86.27	-85.55	-80.91	-82.16	-82.52
Sub-group 2	-86.15	-86.40	-86.89	-85.71	-87.19	-86.21	-82.03	-81.55	-79.18

TABLE X: Parameters extracted from BMI categories sub-groups

Review Board (IRB) for granting the permission to conduct the experiment.

REFERENCES

[1] S. Sangodoyin and A. F. Molisch, "Body Mass Index Effect on Ultrawideband MIMO BAN Channel Characterization," *accepted at Vehicular Technology conference (VTC) 2017, Toronto, Canada*.

[2] ——, "Capacity Measurements for Body Mass Index Dependent Ultrawideband MIMO BAN Channels," *Accepted at Globecom 2017*.

[3] E. Jovanov and A. Milenkovic, "Body area networks for ubiquitous healthcare applications: Opportunities and challenges," *J Med Syst*, vol. 35, pp. 1245–1254, Oct. 2011.

[4] M. Win and R. Scholtz, "Impulse radio: how it works," *Communications Letters, IEEE*, vol. 2, no. 2, pp. 36–38, 1998.

[5] Win, M.Z. and Xiaoxin Qiu and Scholtz, R.A. and Li, V.O.-K., "ATM-based TH-SSMA network for multimedia PCS," *Selected Areas in Communications, IEEE Journal on*, vol. 17, no. 5, pp. 824–836, 1999.

[6] G. Weeks, J. Townsend, and J. Freebersyser, "Performance of hard decision detection for impulse radio," in *Military Communications Conference Proceedings, 1999. MILCOM 1999. IEEE*, vol. 2, 1999, pp. 1201–1206 vol.2.

[7] C. Le Martret and G. Giannakis, "All-digital PAM impulse radio for multiple-access through frequency-selective multipath," in *Global Telecommunications Conference, 2000. GLOBECOM '00. IEEE*, vol. 1, 2000, pp. 77–81 vol.1.

[8] Di Benedetto, M.G. and Giancola, G., *Understanding Ultra Wide Band Radio Fundamentals*, ser. Prentice Hall communications engineering and emerging technologies series. Pearson Education, 2004.

[9] "First report and order 02-48," Federal Communications Commission, Tech. Rep., 2002.

[10] Sahinoglu, Zafer and Gezici, Sinan and Guvenc, Ismail, *Ultra-wideband Positioning Systems: Theoretical Limits, Ranging Algorithms, and Protocols*. New York, NY, USA: Cambridge University Press, 2011.

[11] W. Chang et al, "Frequency-Space-Polarization on UWB MIMO Performance for Body Area Network Applications," *IEEE Antennas and Wireless Propagation Letters*, vol. 7, pp. 577–580, May 2008.

[12] S. V. Roy, et al., "Propagation Modeling for UWB Body Area Networks: Power Decay and Multi-Sensor Correlations," in *10th International Symposium on Spread Spectrum Techniques and Applications*, Bologna, Italy, Aug 2008, pp. 649–653.

[13] D. Cassioli, M. Win, and A. Molisch, "The ultra-wideband bandwidth indoor channel:from statistical models to simulations," *IEEE J. Sel. Areas Commun.*, vol. 20, pp. 1247–1257, Aug 2002.

[14] C.-C. Chong and S. K. Yong, "A generic statistical-based UWB channel model for high-rise apartments," *Antennas and Propagation, IEEE Transactions on*, vol. 53, no. 8, pp. 2389–2399, 2005.

[15] C.-C. Chong, Y.-E. Kim, S. K. Yong, and S.-S. Lee, "Statistical characterization of the UWB propagation channel in indoor residential environment," *Wireless Communications and Mobile Computing*, vol. 5, no. 5, pp. 503–512, 2005. [Online]. Available: http://dx.doi.org/10.1002/wcm.310

[16] Qiu, R.C., "A generalized time domain multipath channel and its application in ultra-wideband (UWB) wireless optimal receiver design-Part II: physics-based system analysis," *Wireless Communications, IEEE Transactions on*, vol. 3, no. 6, pp. 2312–2324, Nov 2004.

[17] Kunisch, Jürgen and Pamp, Jörg, "Measurement results and modeling aspects for the UWB radio channel," in *Ultra Wideband Systems and Technologies, 2002. Digest of Papers. 2002 IEEE Conference on*. IEEE, 2002, pp. 19–23.

[18] Poon, A.S.Y. and Ho, M., "Indoor multiple-antenna channel characterization from 2 to 8 GHz," in *Communications, 2003. ICC '03. IEEE International Conference on*, vol. 5, May 2003, pp. 3519–3523 vol.5.

[19] A. F. Molisch, "Ultrawideband propagation channels-theory, measurement, and modeling," *IEEE Transactions on Vehicular Technology*, vol. 54, pp. 1528–1545, Sep. 2005.

[20] Q. H. Abbasi, et al, "Numerical characterization and modeling of subject-specific ultrawideband body-centric radio channels and systems for healthcare applications," *IEEE Transactions on Information Technology in Biomedicine*, vol. 16, pp. 221–227, Mar. 2012.

[21] A. Keys, F. Fidanza, M. J. Karvonen, N. Kimura, and H. L. Taylor, "Indices of relative weight and obesity," *Journal of Chronic Diseases*, vol. 25, no. 6, pp. 329 – 343, 1972.

[22] N. MacKay, "Scaling of human body mass with height: The body mass index revisited," *Journal of Biomechanics*, vol. 43, no. 4, pp. 764 – 766, 2010. [Online]. Available: http://www.sciencedirect.com/science/article/pii/S0021929009006253

[23] G. Roqueta and A. Fort and C. Craeye and C. Oestges, "Analytical Propagation Models for Body Area Networks," in *Antennas and Propagation for Body-Centric Wireless Communications, 2007 IET Seminar on*, April 2007, pp. 90–96.

[24] T. Alves and B. Poussot and J. M. Laheurte, "Analytical Propagation Modeling of BAN Channels Based on the Creeping-Wave Theory," *IEEE Transactions on Antennas and Propagation*, vol. 59, no. 4, pp. 1269–1274, April 2011.

[25] G. A. Conway and W. G. Scanlon and S. L. Cotton and M. J. Bentum, "An analytical path-loss model for on-body radio propagation," in *Electromagnetic Theory (EMTS), 2010 URSI International Symposium on*, Aug 2010, pp. 332–335.

[26] R. Chandra and A. J. Johansson, "An Analytical Link-Loss Model for On-Body Propagation Around the Body Based on Elliptical Approximation of the Torso With Arms' Influence Included," *IEEE Antennas and Wireless Propagation Letters*, vol. 12, pp. 528–531, 2013.

[27] ——, "A Link Loss Model for the On-Body Propagation Channel for Binaural Hearing Aids," *IEEE Transactions on Antennas and Propagation*, vol. 61, no. 12, pp. 6180–6190, Dec 2013.

[28] A. Fort and F. Keshmiri and G. R. Crusats and C. Craeye and C. Oestges, "A Body Area Propagation Model Derived From Fundamental Principles: Analytical Analysis and Comparison With Measurements," *IEEE Transactions on Antennas and Propagation*, vol. 58, no. 2, pp. 503–514, Feb 2010.

[29] J. Ryckaert and P. De Doncker and R. Meys and A. de Le Hoye and S. Donnay, "Channel model for wireless communication around human body," *Electronics Letters*, vol. 40, no. 9, pp. 543–544, April 2004.

[30] L. Roelens, S. V. den Bulcke, W. Joseph, G. Vermeeren, and L. Martens, "Path loss model for wireless narrowband communication above flat phantom," *Electronics Letters*, vol. 42, no. 1, pp. 10–11–, Jan 2006.

[31] M. Kim and J. I. Takada, "Statistical Model for 4.5-GHz Narrowband On-Body Propagation Channel With Specific Actions," *IEEE Antennas and Wireless Propagation Letters*, vol. 8, pp. 1250–1254, 2009.

[32] P. S. Hall and Y. Hao and Y. I. Nechayev and A. Alomainy and C. C. Constantinou and C. Parini and M. R. Kamarudin and T. Z. Salim and D. T. M. Hee and R. Dubrovka and A. S. Owadally and W. Song and A. Serra and P. Nepa and M. Gallo and M. Bozzetti, "Antennas and propagation for on-body communication systems," *IEEE Antennas and Propagation Magazine*, vol. 49, no. 3, pp. 41–58, June 2007.

[33] A. Fort and C. Desset and P. Wambacq and L. V. Biesen, "Indoor body-area channel model for narrowband communications," *IET Microwaves, Antennas Propagation*, vol. 1, no. 6, pp. 1197–1203, Dec 2007.

[34] S. L. Cotton and W. G. Scanlon, "Characterization of the on-body channel in an outdoor environment at 2.45 GHz," in *2009 3rd European Conference on Antennas and Propagation*, March 2009, pp. 722–725.

[35] A. Fort, P. Doncker, and L. V. Biesen, "An Ultra-Wideband Body Area Propagation Channel Model-From Statistics to Implementation," *IEEE Transactions on Microwave Theory and Techniques*, vol. 54, pp. 1820–1826, Apr 2006.

[36] T. Kobayashi, "Recent progress of ultra wideband radio propagation studies for body area network," in *2009 2nd International Symposium on Applied Sciences in Biomedical and Communication Technologies*, Nov 2009, pp. 1–6.

[37] T. Zasowski and F. Althaus and M. Stager and A. Wittneben and G. Troster, "UWB for noninvasive wireless body area networks: channel measurements and results," in *Ultra Wideband Systems and Technologies, 2003 IEEE Conference on*, Nov 2003, pp. 285–289.

[38] T. Kumpuniemi and T. Tuovinen and M. Hmlinen and K. Y. Yazdandoost and R. Vuohtoniemi and J. Iinatti, "Measurement-based on-body path loss modelling for UWB WBAN communications," in *Medical Information and Communication Technology (ISMICT), 2013 7th International Symposium on*, March 2013, pp. 233–237.

[39] G. Tiberi, N. Ghavami, D. J. Edwards, and A. Monorchio, ""UWB body area network channel modeling: An analytical approach "," *"AEU-International Journal of Electronics and Communications "*, vol. 66, no. 11, pp. 913 – 919, 2012. [Online]. Available: http://www.sciencedirect.com/science/article/pii/S1434841112000696

[40] R. Di Bari and Q. H. Abbasi and A. Alomainy and Y. Hao, "An Advances UWB Channel model for body-centric wireless networks," in *Prog. Electromagn. Res.*, 2013, pp. 77–99.

[41] Xinlei Chen and Xiyu Lu and Depeng Jin and Li Su and Lieguang Zeng, "Channel Modeling of UWB-Based Wireless Body Area Networks," in *IEEE International Conference on Communications*, vol. 6, 2011, pp. 1–9.

[42] M. M. Khan, M. A. Rahman, A. Alomainy, and C. Parini, "Ultra wideband on-body radio radio propagation channels study for different real human test subjects with various sizes and shapes," in *Advances in Electrical Engineering (ICAEE), 2013 International Conference on*, Dec 2013, pp. 323–328.

[43] F. D. Franco, C. Tachtatzis, B. Graham, M. Bykowski, D. C. Tracey, N. F. Timmons, and J. Morrison, "The effect of body shape and gender on wireless body area network on-body channels," in *Antennas and Propagation (MECAP), 2010 IEEE Middle East Conference on*, Oct 2010, pp. 1–3.

[44] M. Qaraqe and Q. H. Abbasi and A. Alomainy and E. Serpedin, "Experimental Evaluation of MIMO Capacity for Ultrawideband Body-Centric Wireless Propagation Channels," *IEEE Antennas and Wireless Propagation Letters*, vol. 13, pp. 495–498, 2014.

[45] Q. H. Abbasi and M. U. Rehman and S. Liaqat and A. Alomainy, "Multiple input multiple output radio channel characterisation for ultra wideband body centric wireless communication," in *2013 IEEE International RF and Microwave Conference (RFM)*, Dec 2013, pp. 238–242.

[46] D. B. Smith, L. W. Hanlen, J. A. Zhang, D. Miniutti, D. Rodda, and B. Gilbert, "First- and second-order statistical characterizations of the dynamic body area propagation channel of various bandwidths," *annals of telecommunications - annales des télécommunications*, vol. 66, no. 3, pp. 187–203, Apr 2011. [Online]. Available: https://doi.org/10.1007/s12243-010-0233-8

[47] D. B. Smith, D. Miniutti, and L. W. Hanlen, "Characterization of the body-area propagation channel for monitoring a subject sleeping," *IEEE Transactions on Antennas and Propagation*, vol. 59, no. 11, pp. 4388–4392, Nov 2011.

[48] D. B. Smith and D. Miniutti, "Cooperative body-area-communications: First and second-order statistics with decode-and-forward," in *2012 IEEE Wireless Communications and Networking Conference (WCNC)*, April 2012, pp. 689–693.

[49] V. G. Chaganti, D. B. Smith, and L. W. Hanlen, "Second-order statistics for many-link body area networks," *IEEE Antennas and Wireless Propagation Letters*, vol. 9, pp. 322–325, 2010.

[50] D. Smith, L. Hanlen, D. Rodda, B. Gilbert, J. Dong, and V. Chaganti, "Body area network radio channel measurement set. v1. CSIRO. Data Collection." https://doi.org/10.4225/08/5947409d34552, accessed: 2018-02-26.

[51] UltRa Lab, "Ultra-wideband radio laboratory," *University of Southern California, Los Angeles, CA*. [Online]. Available: http://ultra.usc.edu/

[52] X. S. Yang and J. Salmi and A. F. Molisch and S. G. Qiu and S. Sangodoyin and B. Z. Wang, "Trapezoidal monopole antenna and array for UWB-MIMO applications," in *2012 International Conference on Microwave and Millimeter Wave Technology (ICMMT)*, vol. 1, May 2012, pp. 1–4.

[53] "RF switch Specifications." [Online]. Available: http://www.pulsarmicrowave.com/product/switch/SW8RD-13

[54] "BMI Classification by World Health Organization," http://www.who.int/mediacentre/factsheets/fs311/en/, accessed: 2017-9-19.

[55] A. P. Kennedy, J. L. Shea, and G. Sun, "Comparison of the Classification of Obesity by BMI vs. Dual-energy X-ray Absorptiometry in the Newfoundland Population," *Obesity*, vol. 17, no. 11, pp. 2094–2099, 2009. [Online]. Available: http://dx.doi.org/10.1038/oby.2009.101

[56] A. Romero-Corral, V. K. Somers, J. Sierra-Johnson, R. J. Thomas, M. L. Collazo-Clavell, J. Korinek, T. G. Allison, J. A. Batsis, F. H. Sert-Kuniyoshi, and F. Lopez-Jimenez, "Accuracy of body mass index in diagnosing obesity in the adult general population," *Int J Obes*, vol. 32, no. 6, pp. 959–966, 02 2008. [Online]. Available: http://dx.doi.org/10.1038/ijo.2008.11

[57] K. J. Rothman, "BMI-related errors in the measurement of obesity," *Int J Obes*, vol. 32, no. S3, pp. S56–S59, print 0000. [Online]. Available: http://dx.doi.org/10.1038/ijo.2008.87

[58] Daniel J. Green, "Is Body Mass Index Really the Best Measure of Obesity in Individuals," *Journal of the American College of Cardiology*, vol. 53, no. 6, p. 526, 2009. [Online]. Available: http://www.sciencedirect.com/science/article/pii/S0735109708037509

[59] R. P. Gelber, J. M. Gaziano, E. J. Orav, J. E. Manson, J. E. Buring, and T. Kurth, "Measures of obesity and cardiovascular risk among men and women," *Journal of the American College of Cardiology*, vol. 52, no. 8, pp. 605 – 615, 2008. [Online]. Available: http://www.sciencedirect.com/science/article/pii/S0735109708019402

[60] S. E. Litwin, "Which Measures of Obesity Best Predict Cardiovascular Risk? Editorials published in the Journal of the American College of Cardiology reflect the views of the authors and do not necessarily represent the views of JACC or the American College of Cardiology." *Journal of the American College of Cardiology*, vol. 52, no. 8, pp. 616 – 619, 2008. [Online]. Available: http://www.sciencedirect.com/science/article/pii/S0735109708019281

[61] D. B. Smith, D. Miniutti, T. A. Lamahewa, and L. W. Hanlen, "Propagation models for body-area networks: A survey and new outlook," *IEEE Antennas and Propagation Magazine*, vol. 55, no. 5, pp. 97–117, Oct 2013.

[62] N. Chahat and G. Valerio and M. Zhadobov and R. Sauleau, "On-Body Propagation at 60 GHz," *IEEE Transactions on Antennas and Propagation*, vol. 61, no. 4, pp. 1876–1888, April 2013.

[63] A. Molisch and et al., "A comprehensive standardized model for ultrawideband propagation channels," *IEEE Trans. Antennas Propag.*, vol. 54, pp. 3151–3166, Nov 2006.

[64] W. Malik, D. Edwards, and C. Stevens, "Angular-spectral antenna effects in ultra-wideband communications links," *Communications, IEE Proceedings-*, vol. 153, no. 1, pp. 99–106, Feb 2006.

[65] X.-S. Yang, K. T. Ng, S. H. Yeung, and K. F. Man, "Jumping genes multiobjective optimization scheme for planar monopole ultrawideband antenna," *IEEE Transactions on Antennas and Propagation*, vol. 56, pp. 3659–3666, Dec. 2008.

[66] C. Bas and S. Ergen, "Ultra-wideband channel model for intra-vehicular wireless sensor networks beneath the chassis: From statistical model

to simulations," *Vehicular Technology, IEEE Transactions on*, vol. 62, no. 1, pp. 14–25, Jan 2013.

[67] Kunisch, J. and Pamp, J., "Measurement results and modeling aspects for the UWB radio channel," in *Ultra Wideband Systems and Technologies, 2002. Digest of Papers. 2002 IEEE Conference on*, May 2002, pp. 19–23.

[68] A. F. Molisch, K. Balakrishnan, C.-C. Chong, S. Emami, A. Fort, J. Karedal, J. Kunisch, H. Schantz, U. Schuster, and K. Siwiak, "IEEE 802.15. 4a channel model-final report," *IEEE P802*, vol. 15, no. 04, p. 0662, 2004.

[69] K. Haneda, A. Richter, and A. Molisch, "Modeling the frequency dependence of ultra-wideband spatio-temporal indoor radio channels," *Antennas and Propagation, IEEE Transactions on*, vol. 60, no. 6, pp. 2940–2950, June 2012.

[70] J. I. Naganawa and J. i. Takada and T. Aoyagi and M. Kim, "Antenna de-embedding in WBAN channel modeling using spherical wave functions: Transmit antenna model validation," in *2016 10th European Conference on Antennas and Propagation (EuCAP)*, April 2016, pp. 1–4.

[71] J. I. Naganawa and K. Haneda and M. Kim and T. Aoyagi and J. I. Takada, "Antenna De-embedding in FDTD-Based Radio Propagation Prediction by Using Spherical Wave Function," *IEEE Transactions on Antennas and Propagation*, vol. 63, no. 6, pp. 2545–2557, June 2015.

[72] Ghassemzadeh, S.S. and Greenstein, L.J. and Kavcic, A and Sveinsson, T. and Tarokh, V., "UWB indoor path loss model for residential and commercial buildings," in *Vehicular Technology Conference, 2003. VTC 2003-Fall. 2003 IEEE 58th*, vol. 5, Oct 2003, pp. 3115–3119 Vol.5.

[73] B. Donlan, S. Venkatesh, V. Bharadwaj, R. Buehrer, and J.-A. Tsai, "The ultra-wideband indoor channel," in *Vehicular Technology Conference, 2004. VTC 2004-Spring. 2004 IEEE 59th*, vol. 1, May 2004, pp. 208–212 Vol.1.

[74] L. J. Greenstein, V. Erceg, Y. Shuan, and M. Clark, "A new path-gain/delay-spread propagation model for digital cellular channels," *IEEE Trans. Vehicular Techn.*, vol. 46, pp. 477–485, May 1997.

[75] S. Sangodoyin, S. Niranjayan, and A. F. Molisch, "A Measurement-Based Model for Outdoor Near-Ground Ultrawideband Channels," *IEEE Transactions on Antennas and Propagation*, vol. 64, no. 2, pp. 740–751, Feb 2016.

[76] J. Karedal, A. J. Johansson, F. Tufvesson, and A. F. Molisch, "A Measurement-Based Fading Model for Wireless Personal Area Networks," *IEEE Transactions on Wireless Communications*, vol. 7, no. 11, pp. 4575–4585, November 2008.

[77] S. Sangodoyin and A. F. Molisch, "Experimental Characterization of the Dependence of UWB Personal Area Networks Channels on Body Mass Index," *accepted to ICC 2018*.

[78] S. L. Cotton and W. G. Scanlon, "A statistical analysis of indoor multipath fading for a narrowband wireless body area network," in *2006 IEEE 17th International Symposium on Personal, Indoor and Mobile Radio Communications*, Sept 2006, pp. 1–5.

[79] ——, "Characterization and modeling of on-body spatial diversity within indoor environments at 868 MHz," *IEEE Transactions on Wireless Communications*, vol. 8, no. 1, pp. 176–185, Jan 2009.

[80] J. Karedal, S. Wyne, P. Almers, F. Tufvesson, and A. F. Molisch, "A measurement-based statistical model for industrial ultra-wideband channels," *Wireless Communications, IEEE Transactions on*, vol. 6, no. 8, pp. 3028–3037, 2007.

[81] S. Sangodoyin and R. He and A. F. Molisch and V. Kristem and F. Tufvesson, "Ultrawideband MIMO Channel Measurements and Modeling in a Warehouse Environment," in *2015 IEEE International Conference on Communications (ICC)*, June 2015, pp. 2277–2282.

[82] P. Tang, J. Zhang, A. Molisch, P. Smith, M. Shafi, and L. Tian, "Estimation of the Ricean K-factor for Wideband Channel Fading," *submitted*.

[83] L. J. Greenstein and S. S. Ghassemzadeh and V. Erceg and D. G. Michelson, "Ricean K-Factors in Narrow-Band Fixed Wireless Channels: Theory, Experiments, and Statistical Models," *IEEE Transactions on Vehicular Technology*, vol. 58, no. 8, pp. 4000–4012, Oct 2009.

[84] A. Molisch, *Wireless Communications*, ser. 2nd ed. Wiley - IEEE. Wiley, 2010.

[85] D. Chizhik, J. Ling, P. W. Wolniansky, R. A. Valenzuela, N. Costa, and K. Huber, "Multiple-input-multiple-output measurements and modeling in manhattan," *IEEE Journal on Selected Areas in Communications*, vol. 21, no. 3, pp. 321–331, Apr 2003.

[86] J. P. Kermoal and L. Schumacher and K. I. Pedersen and P. E. Mogensen and F. Frederiksen, "A stochastic MIMO radio channel model with experimental validation," *IEEE Journal on Selected Areas in Communications*, vol. 20, no. 6, pp. 1211–1226, Aug 2002.

[87] H. Bolcskei, D. Gesbert, and A. J. Paulraj, "On the capacity of ofdm-based spatial multiplexing systems," *IEEE Transactions on Communications*, vol. 50, no. 2, pp. 225–234, Feb 2002.

[88] P. L. Kafle and A. Intarapanich and A. B. Sesay and J. Mcrory and R. J. Davies, "Spatial correlation and capacity measurements for wideband MIMO channels in indoor office environment," *IEEE Transactions on Wireless Communications*, vol. 7, no. 5, pp. 1560–1571, May 2008.

[89] S. Ross, *Simulation*. Academic Press, 2013.